8. J. Benhelm, G. Kirchmair, C. F. Roos, R. Blatt, *Nat. Phys.* **4**, 463 (2008).
9. D. J. Wineland *et al.*, *J. Res. Natl. Inst. Stand. Technol.* **103**, 259 (1998).
10. R. B. Blakestad *et al.*, *Phys. Rev. Lett.* **102**, 153002 (2009).
11. A. Barenco *et al.*, *Phys. Rev. A* **52**, 3457 (1995).
12. M. D. Barrett *et al.*, *Nature* **429**, 737 (2004).
13. A. Sørensen, K. Mølmer, *Phys. Rev. A* **62**, 022311 (2000).
14. C. Langer *et al.*, *Phys. Rev. Lett.* **95**, 060502 (2005).
15. M. D. Barrett *et al.*, *Phys. Rev. A* **68**, 042302 (2003).
16. H. Rohde *et al.*, *J. Opt. B Quantum Semiclass. Opt.* **3**, S34 (2001).
17. B. B. Blinov *et al.*, *Phys. Rev. A* **65**, 040304 (2002).
18. J. P. Home *et al.*, *Phys. Rev. A* **79**, 050305 (2009).
19. M. A. Nielsen, I. L. Chuang, *Quantum Computation and Quantum Information* (Cambridge Univ. Press, Cambridge, 2000).
20. M. Riebe *et al.*, *Phys. Rev. Lett.* **97**, 220407 (2006).
21. J. D. Jost *et al.*, *Nature* **459**, 683 (2009).
22. Material and methods are available as supporting material on *Science* Online.
23. P. J. Lee *et al.*, *J. Opt. B Quantum Semiclass. Opt.* **7**, S371 (2005).
24. N. Lundblad, J. M. Obrecht, I. B. Spielman, J. V. Porto, *arXiv:0902.3213* (2009).
25. G. Kirchmair *et al.*, *Phys. Rev. A* **79**, 020304 (2009).
26. Z. Hradil, J. Řeháček, J. Fiurášek, M. Ježek, *Quantum State Estimation* (Springer-Verlag, 2004), pp. 59–112.
27. M. Horodecki, P. Horodecki, R. Horodecki, *Phys. Rev. A* **60**, 1888 (1999).
28. R. Jozsa, *J. Mod. Opt.* **41**, 2315 (1994).
29. R. Ozeri *et al.*, *Phys. Rev. A* **75**, 042329 (2007).
30. D. L. Moehring *et al.*, *Nature* **449**, 68 (2007).

31. This work was supported by Intelligence Advanced Research Projects Activity and the NIST Quantum Information Program. J.P.H. acknowledges support from a Lindemann Trust Fellowship. We thank E. Knill for helpful discussions, J. J. Bollinger for technical assistance, and Y. Colombe for comments on the manuscript. This paper is a contribution by NIST and not subject to U.S. copyright.

Supporting Online Material

www.sciencemag.org/cgi/content/full/1177077/DC1
Materials and Methods
References

1 June 2009; accepted 8 July 2009
Published online 6 August 2009;
10.1126/science.1177077
Include this information when citing this paper.

A Sulfilimine Bond Identified in Collagen IV

Roberto Vanacore,[1]* Amy-Joan L. Ham,[2]† Markus Voehler,[3] Charles R. Sanders,[2] Thomas P. Conrads,[5]‡ Timothy D. Veenstra,[5] K. Barry Sharpless,[6] Philip E. Dawson,[6,7] Billy G. Hudson[1,2,4]*

Collagen IV networks are ancient proteins of basement membranes that underlie epithelia in metazoa from sponge to human. The networks provide structural integrity to tissues and serve as ligands for integrin cell-surface receptors. They are assembled by oligomerization of triple-helical protomers and are covalently crosslinked, a key reinforcement that stabilizes networks. We used Fourier-transform ion cyclotron resonance mass spectrometry and nuclear magnetic resonance spectroscopy to show that a sulfilimine bond (-S=N-) crosslinks hydroxylysine-211 and methionine-93 of adjoining protomers, a bond not previously found in biomolecules. This bond, the nitrogen analog of a sulfoxide, appears to have arisen at the divergence of sponge and cnidaria, an adaptation of the extracellular matrix in response to mechanical stress in metazoan evolution.

Collagen IV networks are ancient proteins of basement membranes, a specialized form of extracellular matrix, that underlie epithelia in metazoa from sponge to human. The networks confer structural integrity to tissues; serve as scaffolds for the assembly of other macromolecular components; and serve as ligands for integrin cell-surface receptors that mediate cell adhesion, migration, growth, and differentiation (*1*–*3*). The networks participate in signaling events in *Drosophila* development (*4*) and in the clustering of receptors in the development of mammalian neuromuscular junction (*5*), and they are involved in autoimmune and genetic diseases (*6*–*8*). The networks are assembled by oligomerization of triple-helical protomers by end-to-end associations and by intertwining of triple helices (*9*, *10*). At the C terminus, two protomers associate through their trimeric noncollagenous (NC1) domains, forming a hexamer structure. The protomer-protomer interface is covalently crosslinked, a key reinforcement that strengthens the structural integrity of networks. In the case of humans, the crosslink also confers immune privilege to the collagen IV antigen of Goodpasture autoimmune disease (*11*, *12*).

The chemical nature of these crosslinks has been the subject of numerous investigations for 2 decades; yet, the identity of the covalent bond has remained unknown. Initially, the crosslinks were identified as disulfide bonds (*13*), which were subsequently ruled out by the x-ray crystal structure of NC1 hexamers (*14*, *15*). Electron density maps suggested connectivity between methionine-93 (Met^{93}) and lysine-211 (Lys^{211}) at the interface of adjoining protomers (*15*); however, the connectivity is gradually degraded by x-rays, rendering precise characterization a challenge for structural analysis by crystallography (*16*, *17*). By using mass spectrometry (MS) analyses of crosslinked tryptic (Tp) peptides and smaller crosslinked post-proline endopeptidase (PPE) peptides, both derived from the α1α2α1 collagen IV network of placenta, we found that Lys^{211} is modified to hydroxylysine (Hyl^{211}) and that Hyl^{211} is covalently linked to Met^{93}, forming a *S*-hydroxylysyl-methionine (sHM) crosslink (*18*). In the α3α4α5 network (*11*), we found that the sHM crosslink connects the α3 and α5 NC1 domains but that the α4 NC1 domains are connected by a *S*-lysyl-methionine crosslink involving Lys^{211} instead of Hyl^{211}, indicating that this posttranslational modification is not a requirement for crosslink formation (*11*). The nature of the bond linking Met^{93} and Hyl^{211} could not be determined at that time because the observed difference of one mass unit between the uncrosslinked and crosslinked peptides fell within experimental error.

Herein, we deduce the chemical nature of the bond by using Fourier transform ion cyclotron resonance (FTICR) MS (*19*), which can achieve very high mass accuracy [e.g., < 2 parts per million (ppm), about ±0.001 mass units for a peptide with a mass of ~5000], and nuclear magnetic resonance (NMR) spectroscopy to

Table 1. Mass values for the crosslinked Tp peptides from the α1NC1-α1NC1 dimer. The average of the observed peptide mass is indicated with an asterisk.

Z	Theoretical mass	Observed ion (*m/z*)	Observed peptide mass	Difference (theo. − obs.)
+4		1253.6204	5010.473 ± 0.008	
+5		1003.1014	5010.483 ± 0.022	
+6		836.0806	5010.459 ± 0.009	
	5012.488		5010.471 ± 0.022*	2.017

[1]Division of Nephrology, Department of Medicine and Center for Matrix Biology, Vanderbilt University, Nashville, TN 37232, USA. [2]Department of Biochemistry, Vanderbilt University, Nashville, TN 37232, USA. [3]Department of Chemistry, Vanderbilt University, Nashville, TN 37232, USA. [4]Department of Pathology, Vanderbilt University, Nashville, TN 37232, USA. [5]Laboratory of Proteomics and Analytical Technologies, Advanced Technology Program, SAIC-Frederick, Incorporated, National Cancer Institute, Frederick, MD 21702, USA. [6]Department of Chemistry and The Skaggs Institute for Chemical Biology, The Scripps Research Institute, La Jolla, CA 92037, USA. [7]Department of Cell Biology, The Scripps Research Institute, La Jolla, CA 92037, USA.

*To whom correspondence should be addressed. E-mail: roberto.vanacore@vanderbilt.edu (R.V.); billy.hudson@vanderbilt.edu (B.G.H.)

†Present address: Jim Ayers Institute for Precancer Detection and Diagnosis, Vanderbilt University School of Medicine, Nashville, TN 37232, USA.

‡Present address: Department of Pharmacology, University of Pittsburgh School of Medicine, Pittsburgh, PA 15213, USA.

Downloaded from www.sciencemag.org on February 1, 2015

analyze crosslinked Tp peptides derived from the α1NC1-α1NC1 dimer. Table 1 shows the mass values for the multiple-charge states (+4, +5, and +6) of the crosslinked Tp peptide. For each charge state, 10 consecutive scans were averaged to obtain the observed monoisotopic mass value of 5010.471 ± 0.022 (SEM) (Table 1). This value is 2.017 mass units lower than the theoretical total mass (5012.486) of the two constituent tryptic peptides, a Met^{93}-containing peptide (T-3599.688) and a Hyl^{211}-containing peptide (T-1412.777), which were previously described (*18*).

To determine the location of modifications that lead to the loss of 2.017 mass units, we analyzed the tryptic complex by collision-induced dissociation (CID) MS^3 (MS/MS/MS) fragmentation analysis. The mass-to-charge ratio (*m/z*) of 1003.1014 (+5) ion was selected for MS^2 fragmentation, which generated a *m/z* = 730.399 ion, corresponding to the T-1412.799 peptide plus 45.984 mass units, and a *m/z* = 1184.900 ion, corresponding to the T-3599.689 peptide that lost 48.013 mass units (Fig. 1A). To locate these mass changes to specific residues, we selected the *m/z* = 730.3994 and *m/z* = 1184.900 ions for further CID (MS^3). The y and b series of the spectra confirm not only the sequence of the T-1412.799 peptide but also that the location of the mass change of +45.984 corresponds to the side chain of Hyl^{211} (fig. S1A). The MS^3 fragmentation profile for the *m/z* = 1184.900 ion also verified the peptide sequence and localized the loss of 48.013 mass units to Met^{91} or Met^{93} (fig. S1B). A smaller crosslinked PPE peptide complex derived from the crosslinked Tp peptides (fig. S2) confirmed that the loss of 48.013 mass units is localized to the side chain of Met^{93}. An analogous fragmentation has been observed in methionine sulfoxide–containing peptides that undergo concomitant neutral loss of methane sulfenic acid (CH_3SOH) (*20*, *21*). In this case, however, this group remains attached to the side chain of Hyl^{211}, demonstrating the covalent nature of the interaction between Met^{93} and Hyl^{211}. These findings for the crosslink in the α1NC1-α1NC1 dimer are identical to that for the α2NC1-α2NC1 dimer (fig. S3).

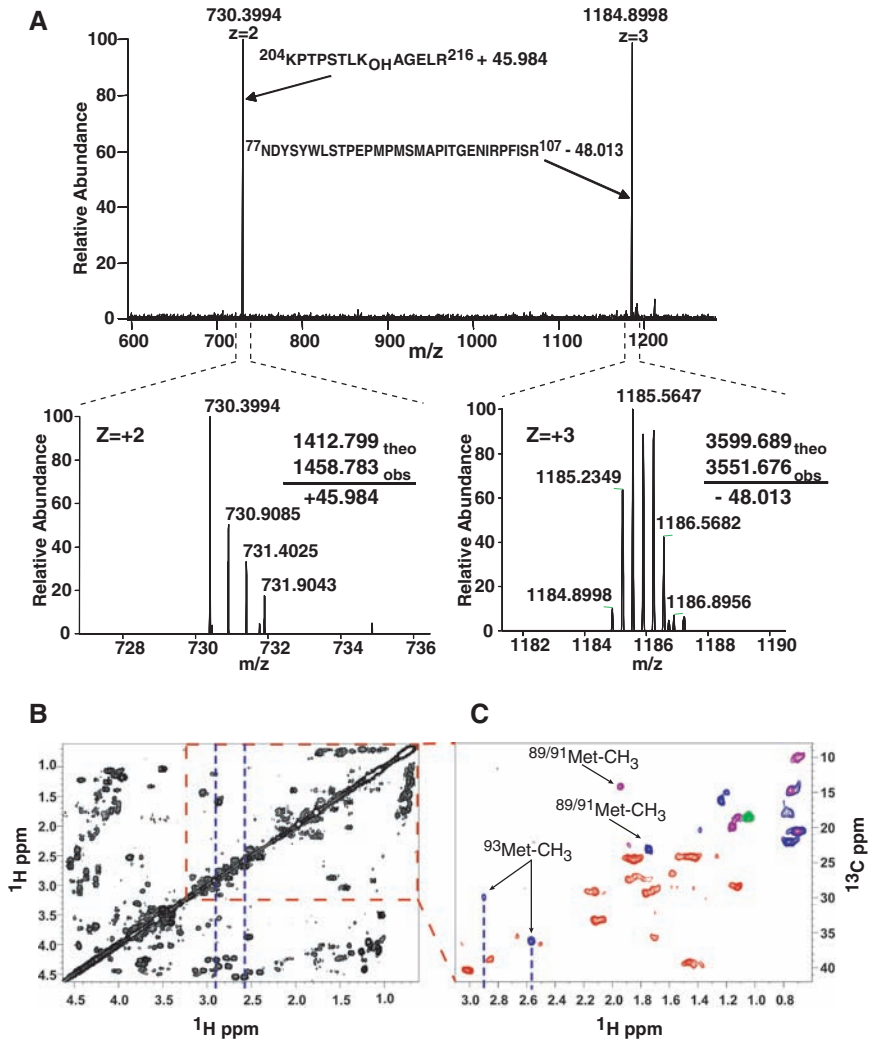

Fig. 1. Mass spectrometric and NMR analyses of the crosslinked Tp peptides from the α1NC1-α1NC1 dimer. (**A**) MS^2 spectrum showing the fragmentation by CID of the *m/z* = 1003.1014 (+5) ion (Table 1). The bottom graphs show the isotopic envelope for each ion and the mass difference of each fragment with respect to the uncrosslinked peptides. (**B**) NMR studies showing the ^1H-^1H COSY spectrum in 50 mM phosphate buffer, pH = 7.0, 20°C. (**C**) Edited ^1H-^{13}C HSQC spectrum of an expanded portion of (B) in which the methyl groups of Val, Leu, Thr, Iso, and Met are expected. Correlation peaks are color-coded according to multiplicity edited HSQC spectra, optimized for correlation selection of CH_2 (red), CH/CH_3 (blue), and CH (green) only. Several peaks contain overlapping signals from CH_3 and CH groups and are indicated in purple.

An overlay of correlation spectroscopy (COSY) and heteronuclear multiple quantum correlation (^1H-^{13}C HMQC) spectra of the crosslinked Tp peptides was used to evaluate the chemical shift of the methyl group of Met^{93} (Fig. 1B and fig. S4A). The sequences of crosslinked Tp peptides have a total of 25 methyl groups, three of which belong to Met^{89}, Met^{91}, and Met^{93}. Typical proton chemical shift for methyl groups in peptides of Leu, Thr, Iso, and Ala is between 0 and 1.5 ppm and that of Met is about 2.1 ppm. Eighteen out of 22 total methyl groups of Leu, Thr, Ile, and Ala were identified within the expected chemical shift range in the HMQC spectrum (fig. S4B). An edited heteronuclear single quantum correlation (HSQC) analysis was carried out to identify the methyl groups of Met^{89}, Met^{91}, and Met^{93}. In the chemical shift range expected for Met, two signals were observed: one at ^1H 1.9 ppm/^{13}C 14 ppm and the other at ^1H 1.7/^{13}C 24 ppm, presumably corresponding to Met^{89} and/or Met^{91} (Fig. 1C). In addition, two downfield-shifted methyl resonances were observed that had atypical chemical shifts at ^1H 2.9 ppm/^{13}C 30 ppm and ^1H 2.6ppm/^{13}C 36 ppm. These features likely correspond to the methyl group of Met^{93} in two different chemical environments, such as cyclic or alternate chiral forms of the crosslink (fig. S5).

The collective evidence from the MS and NMR indicates the existence of a sulfilimine bond in the crosslinked Tp peptides (Fig. 2A). MS analysis revealed that the linkage between Met^{93} and Hyl^{211} is characterized by the loss of two hydrogen atoms, which is consistent with oxidation resulting in a double bond that connects the sulfur atom of Met^{93} and the nitrogen atom of Hyl^{211} (Fig. 2A). The MS^2 fragmentation of the tryptic complex can be explained by a concerted process in which a β-hydrogen is taken up by the nitrogen, which leads to the cleavage of the bond between sulfur and γ-carbon of Met^{93} (Cope elimination) (*22*). This syn elimination is also observed in the fragmentation of methionine sulfoxide and is analogous to the Cope elimination of amine oxides. The resulting products, an olefin fragment and a methylsulfenamide fragment, are shown in Fig. 2A. The sulfilimine structure is further supported by a down-shifted methyl peak in the NMR spectrum of the crosslinked Tp peptides, which is consistent with the shift of the methyl group of *S*-methylisothiazolidinium nitrate (^1H 2.78 ppm).

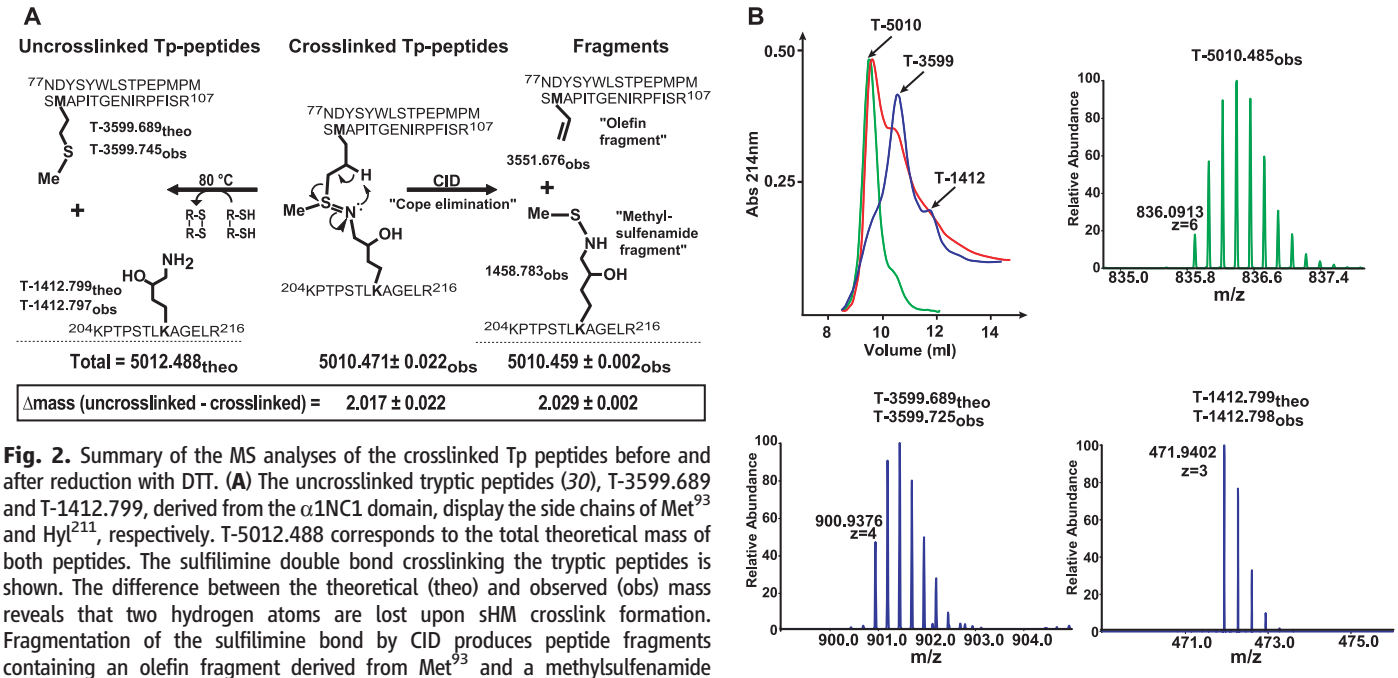

Fig. 2. Summary of the MS analyses of the crosslinked Tp peptides before and after reduction with DTT. (**A**) The uncrosslinked tryptic peptides (*30*), T-3599.689 and T-1412.799, derived from the α1NC1 domain, display the side chains of Met^{93} and Hyl^{211}, respectively. T-5012.488 corresponds to the total theoretical mass of both peptides. The sulfilimine double bond crosslinking the tryptic peptides is shown. The difference between the theoretical (theo) and observed (obs) mass reveals that two hydrogen atoms are lost upon sHM crosslink formation. Fragmentation of the sulfilimine bond by CID produces peptide fragments containing an olefin fragment derived from Met^{93} and a methylsulfenamide fragment derived from Hyl^{211} as a result of the Cope elimination event in the gas phase. However, chemical reduction with DTT, formally involving addition of two H atoms, severs the sulfilimine link and recovers Met^{93} and Hyl^{211}, as indicated below. (**B**) Crosslinked Tp peptides were separated by gel filtration chromatography before (green) and after incubation in 100 mM DTT at room temperature (red) and 80°C (blue). The arrows indicate the identity of each chromatographic peak as revealed by MS analysis.

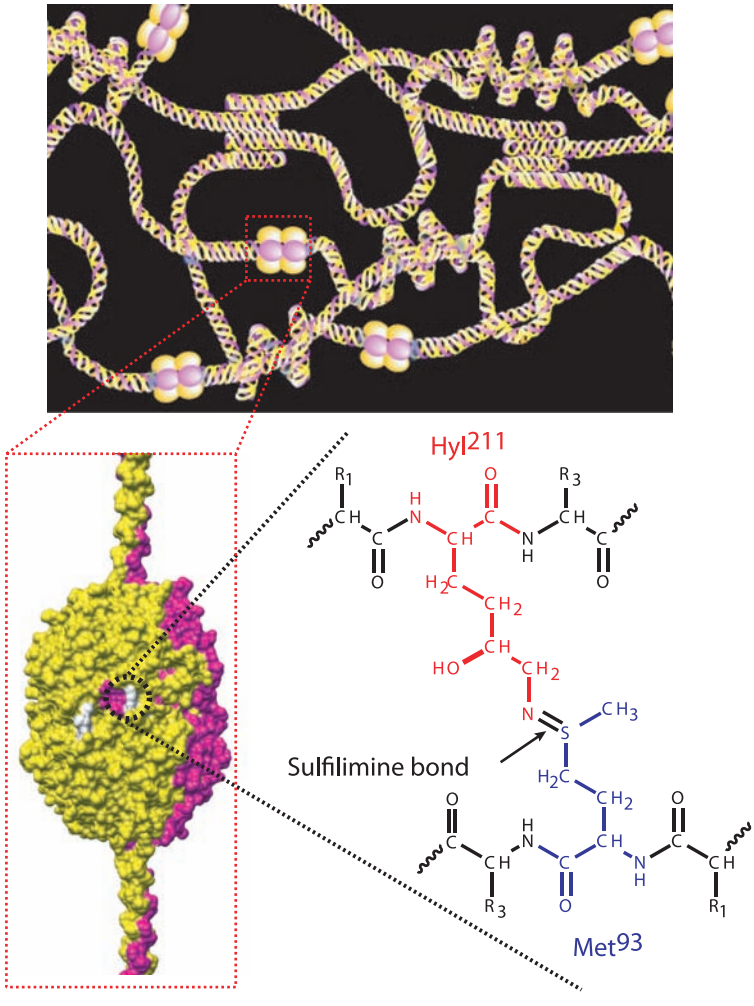

Fig. 3. Proposed chemical structure of the sHM crosslink. (**Top**) Schematic of the α1α2α1 collagen IV network illustrating the interaction between the NC1 domains of triple-helical protomers. (**Bottom left**) A space-filling model of the NC1 hexamer quaternary structure shows the location of the sHM crosslinks (white). The sulfilimine bond that constitutes the sHM crosslink connecting the side chains of Met^{93} and Hyl^{211} is shown for the α1NC1-α1NC1 dimer (yellow). The same bond connects Met^{93} and Hyl^{211} in the α2NC1-α2NC1 dimer (magenta).

Although a sulfilimine bond has not been reported in any native biomolecule, they occur in other molecules (*23*). They are the nitrogen analog of sulfoxides, S(IV), and are also known as sulfur-nitrogen ylides. Most sulfilimines that have been reported are stabilized by strong electron-withdrawing groups on the nitrogen end of the sulfilimine linkage (*24*). However, cyclic sulfilimines derived from the oxidation of methionine analogs by I_2 have been characterized in detail as their isothiazolidinium salts after protonation of the nitrogen (*25*, *26*). These studies showed direct bonding of the nitrogen and sulfur atoms and a new stereogenic center at the sulfur atom, consistent with the two methyl resonances seen by NMR. In the case of collagen IV, sulfilimine crosslinks are likely to be formed through a two-electron, heteroatom transfer class oxidation (*27*). For example, the Met^{93} sulfide could react with a chemical or enzymatic oxidant to form a transient, sulfur-(IV) sulfonium intermediate, which is captured by the Hyl^{211} or Lys^{211} amine to form the sulfilimine. The latter S_N2-like step entails inversion at sulfur because the S-X bond breaks heterolytically and is analogous to the known oxidation of free methionine to dehydromethionine mediated by iodine (*26*). This sulfilimine linkage may not occur only in collagen IV but in other proteins as well.

Sulfilimines are reduced by thiols to yield the parent amine and thioether groups (*23*, *24*). Thus, the susceptibility of the crosslinked Tp peptide to dithiothreitol (DTT) reduction was evaluated (Fig. 2B). Partial reduction was achieved with 100 mM DTT at room temperature and complete reduction at 80°C at pH = 7.8. Mass spectrometry analyses revealed that DTT breaks the crosslink with the concomitant generation of the T-3599 and T-1412 peptides with complete recovery of both Met^{93} and Hyl^{211}, respectively (Fig. 2, A and B). The susceptibility of the crosslink to reduction is comparable to that of disulfide bonds of insulin (fig. S6). Because the crosslinked Tp peptides do not contain cysteines (Fig. 2A), these results provide further support for the existence of a sulfilimine bond between Hyl^{211} and Met^{93}.

The location of the sulfilimine linkage within the α1α2α1 collagen IV network is shown in Fig. 3. Up to six sulfilimine bonds fasten the interface of the trimeric NC1 domains of two adjoining protomers, reinforcing the quaternary structure of the networks. Furthermore, the sulfilimine bond also occurs in the α3α4α5 collagen IV network (fig. S7) because fragmentation pattern of its crosslinked tryptic peptides (*11*) is identical to that of the α1α2α1 network described herein.

The sulfilimine bond likely occurs in diverse metazoan species. NC1 dimer subunits, a signature structural feature indicative of crosslinks, have been identified in collagenase digests of basement membranes including those of human (*28*), bovine (*28*), dog (*29*), and mouse (*28*). Furthermore, a phylogenetic analysis of the Lys^{211} and Met^{93} residues, based on a multiple sequence alignment of the NC1 domain across the metazoan phylum [Fig. 4 and (*30*)], revealed that the sulfilimine bond may occur in many metazoans, except in hydra, flatworm, sponge, and placozoa. A further comparison of the sequence motif [X-K-A, S, or G (*31*)] that confers hydroxylation of lysyl residues by lysyl hydroxylase (*32*) occurs in the NC1 domains of all metazoa except hydra, sponge, and placozoa. The motif is also absent in the α4 NC1 domain of human, mouse, bovine, and chick, which in the case of bovine Lys^{211} does not undergo hydroxylation and leads to the formation of sKM crosslink (*11*). In one species of the phylum cnidaria, *Nematostella vectensis*, Met^{93} and Lys^{211} and the hydroxylation motif of Lys are conserved (Fig. 4), suggesting that the sHM crosslink appeared at the time of the divergence of sponge and cnidaria, an apparent evolutionary adaptation that arose in response to mechanical stress on organisms.

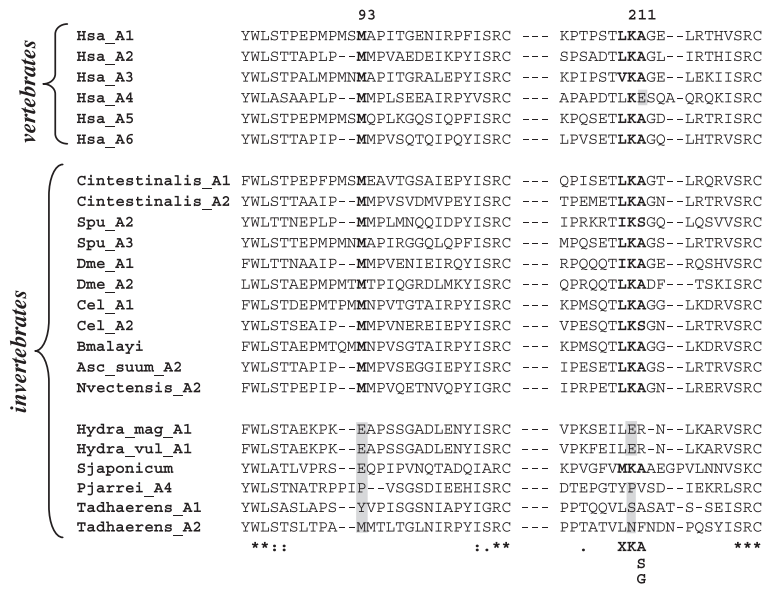

Fig. 4. Multiple sequence alignment of collagen IV NC1 domain sequences encompassing Met^{93} and Lys^{211} (*31*). Met^{93} and Lys^{211} are shown in bold. Conserved amino acid residues are indicated with an asterisk. Semi-conserved residues are indicated with a colon. The hydroxylation motif for lysyl hydroxylase, X-K-(A or S or G) is shown at the bottom of the alignment. Abbreviations are as follows: *Homo sapiens* (Hsa) A1, NP_001836.2; A2, NM_001846.2; A3, ABX71213.1; A4, X81053.1; A5, ABW24668.1; and A6, AL136080.6. *Ciona intestinalis* (Cintestinalis) A1, XP_2120982.1; and A2, XP_2119477.1. *Strongylocentrotus purpuratus* (Spu) A2, NP_999676.1; and A3, NP_999631.1. *Drosophila melanogaster* (Dme) A1, AAA28404.1; and A2, AAB64082.1. *Caenorhabditis elegans* (Cel) A1, AAB59179.1; and A2, AAA27989.1. *Brugia malayi* (Bmalayi) XP_1902932.1. *Ascaris Suum* (Asc_suum) AAA18014.1. *Nematostella vectensis* (Nvectensis) XP_1626265.1. *Hydra magnipapillata* (Hydra_mag) XP_2157001.1. *Hydra vulgaris* (Hydra_vul) AAG40729.1. *Schistosoma japonicum* (Sjaponcum) AAX25734.2. *Trichoplax adhaerens* (Tadhaerens) A1, EDV21329.1; and A2, EDV21231.1. The alignments were generated with ClustalW, www.ebi.ac.uk.Tools/clustalw2/index.html (*33*).

References and Notes

1. M. Moser, K. R. Legate, R. Zent, R. Fässler, *Science* **324**, 895 (2009).
2. R. O. Hynes, *Cell* **110**, 673 (2002).
3. P. D. Yurchenco, H. Furthmayr, *Biochemistry* **23**, 1839 (1984).
4. X. Wang, R. E. Harris, L. J. Bayston, H. L. Ashe, *Nature* **455**, 72 (2008).
5. M. A. Fox *et al.*, *Cell* **129**, 179 (2007).
6. D. B. Gould *et al.*, *N. Engl. J. Med.* **354**, 1489 (2006).
7. D. B. Gould *et al.*, *Science* **308**, 1167 (2005).
8. B. G. Hudson, K. Tryggvason, M. Sundaramoorthy, E. G. Neilson, *N. Engl. J. Med.* **348**, 2543 (2003).
9. J. Khoshnoodi, V. Pedchenko, B. G. Hudson, *Microsc. Res. Tech.* **71**, 357 (2008).
10. J. Khoshnoodi *et al.*, *J. Biol. Chem.* **281**, 6058 (2006).
11. R. M. Vanacore *et al.*, *J. Biol. Chem.* **283**, 22737 (2008).
12. D. B. Borza *et al.*, *J. Biol. Chem.* **280**, 27147 (2005).
13. B. Siebold, R. Deutzmann, K. Kuhn, *Eur. J. Biochem.* **176**, 617 (1988).
14. M. Sundaramoorthy, M. Meiyappan, P. Todd, B. G. Hudson, *J. Biol. Chem.* **277**, 31142 (2002).
15. M. E. Than *et al.*, *Proc. Natl. Acad. Sci. U.S.A.* **99**, 6607 (2002).
16. M. E. Than, G. P. Bourenkov, S. Henrich, K. Mann, W. Bode, *Biol. Chem.* **386**, 759 (2005).
17. R. M. Vanacore *et al.*, *J. Biol. Chem.* **279**, 44723 (2004).
18. R. M. Vanacore, D. B. Friedman, A. J. Ham, M. Sundaramoorthy, B. G. Hudson, *J. Biol. Chem.* **280**, 29300 (2005).
19. Materials and methods are available as supporting material on *Science* Online.
20. F. M. Lagerwerf, M. van de Weert, W. Heerma, J. Haverkamp, *Rapid Commun. Mass Spectrom.* **10**, 1905 (1996).
21. G. E. Reid, K. D. Roberts, E. A. Kapp, R. I. Simpson, *J. Proteome Res.* **3**, 751 (2004).
22. A. Cope, T. Foster, P. Towle, *J. Am. Chem. Soc.* **71**, 3929 (1949).
23. I. V. Koval, *Russ. Chem. Rev.* **59**, 1409 (1990).
24. T. L. Gilchrist, C. J. Moody, *Chem. Rev.* **77**, 409 (1977).
25. D. O. Lambeth, D. Swank, *J. Org. Chem.* **44**, 263 (1979).
26. R. S. Glass, J. R. Duchek, *J. Am. Chem. Soc.* **98**, 965 (1976).
27. C. R. Johnson, C. C. Bacon, W. D. Kingsbur, *Tetrahedron Lett.* **13**, 501 (1972).
28. S. Weber, J. Engel, H. Wiedemann, R. Glanville, R. Timpl, *Eur. J. Biochem.* **139**, 401 (1984).
29. P. S. Thorner, K. Zheng, R. Kalluri, R. Jacobs, B. G. Hudson, *J. Biol. Chem.* **271**, 13821 (1996).

30. A. Aouacheria *et al.*, *Mol. Biol. Evol.* **23**, 2288 (2006).
31. Single-letter abbreviations for the amino acid residues are as follows: A, Ala; C, Cys; D, Asp; E, Glu; F, Phe; G, Gly; H, His; I, Ile; K, Lys; L, Leu; M, Met; N, Asn; P, Pro; Q, Gln; R, Arg; S, Ser; T, Thr; V, Val; W, Trp; X, any amino acid; and Y, Tyr.
32. K. I. Kivirikko, T. Pihlajaniemi, *Adv. Enzymol. Relat. Areas Mol. Biol.* **72**, 325 (1998).
33. M. A. Larkin *et al.*, *Bioinformatics* **23**, 2947 (2007).
34. We thank D. Liebler for facilitating the initial contact with T. D. Veenstra from SAIC-Frederick, Incorporated, and C. Bolm (Aachen University, Germany) for helpful discussions. The technical assistance of P. Todd and M. Rafi is greatly appreciated. We would also like to thank S. Hill and H. McDonald, from the Proteomics Laboratory at the Mass Spectrometry Research Center of Vanderbilt University, for their assistance with the Orbitrap-LTQ (Therme Electron, San Jose, CA) instrument. This work was supported in part by NIH grants DK065123 and DK18381 (to B.G.H.), DC007416 (C.R.S.), and GM059380 (P.E.D.); the W. M. Keck Foundation (K.B.S.); and the Skaggs Institute for Chemical Biology (K.B.S.). R.V. and B.G.H. have filed a provisional patent (1 June 2009) on the potential enzyme system that catalyses the sulfilimine bond formation and that may be involved in pathophysiological processes.

Supporting Online Material
www.sciencemag.org/cgi/content/full/325/5945/1230/DC1
Materials and Methods
Figs. S1 to S7

26 May 2009; accepted 13 July 2009
10.1126/science.1176811

Reassessing the Source of Long-Period Comets

Nathan A. Kaib* and Thomas Quinn

We present numerical simulations to model the production of observable long-period comets (LPCs) from the Oort Cloud, a vast reservoir of icy bodies surrounding the Sun. We show that inner Oort Cloud objects can penetrate Jupiter's orbit via a largely unexplored dynamical pathway, and they are an important, if not the dominant, source of known LPCs. We use this LPC production to place observationally motivated constraints on the population and mass of the inner Oort Cloud, which are consistent with giant planet formation theory. These constraints indicate that only one comet shower producing late Eocene bombardment levels has likely occurred since the Cambrian Explosion, making these phenomena an improbable cause of additional extinction events.

Because of their large distances from the Sun, Oort Cloud bodies undergo orbital evolution driven by gravitational perturbations from passing stars and the galactic tide (*1*, *2*). During this process, semimajor axes (a) remain nearly constant while perihelia (closest approach distances to the Sun, or q) evolve under these perturbations. Although most Oort Cloud bodies have perihelia far outside the planetary region of the Solar System, a tiny fraction are continually injected into planet-crossing orbits (*3*). Once there, they receive energy kicks from planetary perturbations during each perihelion passage, causing the semimajor axes to change at random. The magnitude of these kicks increases greatly near Jupiter and Saturn, and in the inner 10 to 15 astronomical units (AU) of the Solar System the typical planetary energy kick is greater than the gravitational binding energy of Oort Cloud orbits (*4*). Thus, inward perihelion drift of long-period comets (LPCs) is halted inside ~10 to 15 AU because they are either immediately ejected to interstellar space or perturbed onto low-a (and therefore fixed-q) orbits before eventually being ejected. This effect, known as the Jupiter-Saturn barrier, prevents many Oort Cloud bodies from passing near Earth.

To reach an observable orbit ($q < 5$ AU), an Oort Cloud body's perihelion must therefore decrease from outside 10 to 15 AU to inside 5 AU in less than one orbital period. Bodies with $a \lesssim 20{,}000$ AU are less sensitive to galactic perturbations, and, except during rare close stellar passages causing comet showers, their perihelia evolve too slowly to reach observable orbits before ejection. For this reason, the Jupiter-Saturn barrier has traditionally been thought to prevent bodies in the inner 20,000 AU of the Oort Cloud from evolving to currently observable LPCs (*2*), and this has been the motivation for dividing the Oort Cloud into the inner (unobservable) cloud with $a < 20{,}000$ AU and outer (observable) cloud with $a > 20{,}000$ AU. The edge of the Jupiter-Saturn barrier is not abrupt, however, and recent modeling of scattered disk orbits indicates that repeated smaller planetary energy kicks near the barrier edge can inflate low-a orbits to $a > 20{,}000$ AU (*5*).

Here, we present numerical simulations of the production of observable LPCs (*6*), and we find that many observable LPCs ultimately originate from the inner Oort Cloud (Fig. 1). In the case shown here, an inner Oort Cloud body with an initial semimajor axis of 6000 AU had a perihelion slowly evolving Sunward under the influence of the galactic tide. When the perihelion was beyond ~18 AU, the semimajor axis was nearly unaltered by the relatively weak perturbations of Uranus and Neptune. Between 18 and 14 AU, however, a was rapidly inflated to ~30,000 AU. With such a large semimajor axis, the perihelion then decreased by 13 AU during the next orbital period, circumventing the Jupiter-Saturn barrier and evolving to an observable LPC. About 85% of inner Oort Cloud bodies evolving to observable LPCs followed an evolution similar to that shown in Fig. 1. Details of other known minor LPC production pathways that are less direct and efficient (*7*) can be found in the supporting online material (SOM) text.

Although LPC production has been modeled previously, a substantial inner Oort Cloud contribution has hitherto gone unnoticed. In some models, this is because planetary perturbations are not included (*8*, *9*), leaving no mechanism to inflate a near the Jupiter-Saturn barrier. However, some works include the full gravity of the giant planets (*3*, *10*). In these instances, orbital elements of incoming LPCs are sampled when they have already attained $q < 5$ AU, obscuring any prior a evolution. We performed a similar orbit sampling of dynamically new LPCs (LPCs entering the observable region for the first time) (Fig. 2A). The resulting a distribution hides the inner Oort Cloud's contribution.

To assess the inner Oort Cloud's LPC production, we instead considered the initial semimajor axes from which LPCs evolved in our simulation (Fig. 2A). This distribution indicates that just over half of all dynamically new LPCs come from the inner Oort Cloud, which is a conservative estimate because we used an Oort Cloud model with a low inner-to-outer population ratio of 1.5:1 (see SOM text for a treatment of alternative models). Below $a \sim 5000$ AU, LPC production fell dramatically because of the nonisotropic nature of the innermost part of our Oort Cloud model (fewer orbits had decreasing perihelia in this region). However, even additional simulations with a more-isotropized

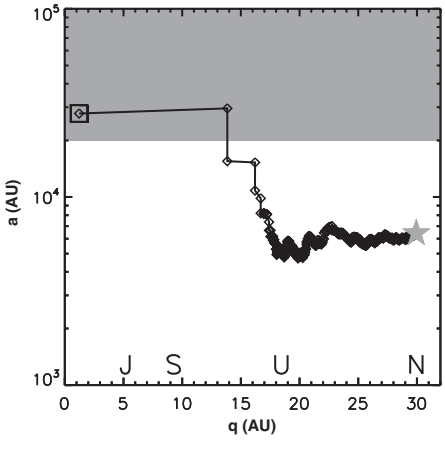

Fig. 1. An example of the typical evolution from an inner Oort Cloud object into an observable LPC. Orbital elements are sampled each time the object crosses the $r = 35$ AU boundary (twice per orbit). The star data point marks the start of the evolution and the square marks the end. The shaded area indicates the a range of the outer Oort Cloud, and the perihelia of the giant planets are noted with their initials.

Department of Astronomy, University of Washington, Box 351580, Seattle, WA 98195–1580, USA.

*To whom correspondence should be addressed. E-mail: kaib@astro.washington.edu

Science
AAAS

A Sulfilimine Bond Identified in Collagen IV

Roberto Vanacore *et al.*

Science **325**, 1230 (2009);
DOI: 10.1126/science.1176811

This copy is for your personal, non-commercial use only.

If you wish to distribute this article to others, you can order high-quality copies for your colleagues, clients, or customers by clicking here.

Permission to republish or repurpose articles or portions of articles can be obtained by following the guidelines here.

The following resources related to this article are available online at www.sciencemag.org (this information is current as of February 1, 2015):

Updated information and services, including high-resolution figures, can be found in the online version of this article at:
http://www.sciencemag.org/content/325/5945/1230.full.html

Supporting Online Material can be found at:
http://www.sciencemag.org/content/suppl/2009/09/03/325.5945.1230.DC1.html

This article **cites 31 articles**, 11 of which can be accessed free:
http://www.sciencemag.org/content/325/5945/1230.full.html#ref-list-1

This article has been **cited by** 2 article(s) on the ISI Web of Science

This article has been **cited by** 11 articles hosted by HighWire Press; see:
http://www.sciencemag.org/content/325/5945/1230.full.html#related-urls

This article appears in the following **subject collections:**
Chemistry
http://www.sciencemag.org/cgi/collection/chemistry

Downloaded from www.sciencemag.org on February 1, 2015

Science (print ISSN 0036-8075; online ISSN 1095-9203) is published weekly, except the last week in December, by the American Association for the Advancement of Science, 1200 New York Avenue NW, Washington, DC 20005. Copyright 2009 by the American Association for the Advancement of Science; all rights reserved. The title *Science* is a registered trademark of AAAS.